

UNCLASSIFIED

AD NUMBER

AD468430

LIMITATION CHANGES

TO:

Approved for public release; distribution is unlimited.

FROM:

Distribution authorized to U.S. Gov't. agencies and their contractors;
Administrative/Operational Use; 15 MAR 1965.
Other requests shall be referred to Bureau of Naval Weapons, Washington, DC 20350.

AUTHORITY

NAVAIR ltr dtd 10 Feb 1975

THIS PAGE IS UNCLASSIFIED

SECURITY

MARKING

The classified or limited status of this report applies to each page, unless otherwise marked.

Separate page printouts MUST be marked accordingly.

THIS DOCUMENT CONTAINS INFORMATION AFFECTING THE NATIONAL DEFENSE OF THE UNITED STATES WITHIN THE MEANING OF THE ESPIONAGE LAWS, TITLE 18, U.S.C., SECTIONS 793 AND 794. THE TRANSMISSION OR THE REVELATION OF ITS CONTENTS IN ANY MANNER TO AN UNAUTHORIZED PERSON IS PROHIBITED BY LAW.

NOTICE: When government or other drawings, specifications or other data are used for any purpose other than in connection with a definitely related government procurement operation, the U. S. Government thereby incurs no responsibility, nor any obligation whatsoever; and the fact that the Government may have formulated, furnished, or in any way supplied the said drawings, specifications, or other data is not to be regarded by implication or otherwise as in any manner licensing the holder or any other person or corporation, or conveying any rights or permission to manufacture, use or sell any patented invention that may in any way be related thereto.

Quarterly Technical Summary Report

December 14, 1964 to March 15, 1965

(Report No. 2 for Contract Period)

(Report No. 14 of Series)

**VISCOELASTIC PROPERTIES OF SOLID PROPELLANTS
AND PROPELLANT BINDERS**

Prepared for:

DEPARTMENT OF THE NAVY
BUREAU OF NAVAL WEAPONS (RMMP-2)
CONTRACT NO. NOW 65-0061-d

Sponsored by:

ADVANCED RESEARCH PROJECTS AGENCY
PROPELLANT CHEMISTRY OFFICE
ARPA ORDER NO. 22, AMENDMENT NO. 74

Qualified requesters may obtain
copies of this report direct from
DDC. Foreign announcement and
dissemination of this report by
DDC is not authorized.

STANFORD RESEARCH INSTITUTE

MENLO PARK, CALIFORNIA

***SRI**

STANFORD RESEARCH INSTITUTE

MENLO PARK, CALIFORNIA



*Quarterly Technical Summary Report
(Report No. 2 for Contract Period)
(Report No. 14 of Series)*

December 16, 1964 to March 15, 1965

VISCOELASTIC PROPERTIES OF SOLID PROPELLANTS AND PROPELLANT BINDERS

Prepared for:

DEPARTMENT OF THE NAVY
BUREAU OF NAVAL WEAPONS (RMMP-2)
CONTRACT NO. NOw 65-0061-d

Sponsored by:

ADVANCED RESEARCH PROJECTS AGENCY
PROPELLANT CHEMISTRY OFFICE
ARPA ORDER NO. 22, AMENDMENT NO. 74

By: NICHOLAS W. TSCHOEGL JAMES R. SMITH THOR L. SMITH

SRI Project PRU-5174

Approved: LIONEL A. DICKINSON, DIRECTOR
POLYMER AND PROPULSION SCIENCES

Copy No. 182.

ABSTRACT

Studies supplementary to the determination of the dynamic shear modulus are reported. The effect of specimen geometry and the magnitude of shear strain on the dynamic modulus of polyurethane propellant AEBA-10 was studied. A method was worked out to correct measurements to the same level of shear strain to allow a direct comparison under all experimental conditions. An evaluation of the differential Lissajous method for determining small phase angles has shown that, at frequencies as low as 0.05 cps, a phase angle of the order of a few thousandths of a radian can be measured with good precision. An evaluation was made of the static compressibility apparatus by determining the compressibility of dioctylsebacate at 25 and 50°C and at pressures up to 2000 psi. The results are in excellent agreement with reported data. Factors that influence the reproducibility of data obtained with the dynamic compressibility apparatus have been investigated.

CONTENTS

ABSTRACT	ii
LIST OF ILLUSTRATIONS.	iv
LIST OF TABLES	v
I INTRODUCTION	1
II DYNAMIC SHEAR PROPERTIES	2
A. Static Shear Modulus of SBR	2
B. Static Shear Modulus of Polyurethane Propellant AEBA-10.	5
C. Effect of Specimen Geometry and Cam Displacement on Dynamic Shear Moduli	7
D. Differential Lissajous Method	9
1. Verification of the Method	10
2. The Role of the Base Gain.	12
III DEPENDENCE OF SPECIFIC VOLUME ON PRESSURE, TEMPERATURE, AND TIME	16
A. Static Compressibility.	16
B. Dynamic Bulk Compressibility.	18

ILLUSTRATIONS

Fig. 1	Plot of Compressive Stress σ_c <u>vs.</u> $-(\lambda - \lambda^{-2})$ for SBR Specimens.	3
Fig. 2	Plot of Compressive Stress σ_c <u>vs.</u> Compressive Strain ϵ_c for Specimens of Polyurethane Propellant AEBA-10. . . .	5
Fig. 3	Shear Strain Dependence of the Storage and Loss Moduli of Polyurethane Propellant AEBA-10 Specimens. Effect of Specimen Thickness	8
Fig. 4	Shear Strain Dependence of the Storage and Loss Moduli of Polyurethane Propellant AEBA-10 Specimens. Effect of Specimen Diameter.	9
Fig. 5	Shear Strain Dependence of the Storage and Loss Moduli of Polyurethane Propellant AEBA-10 Specimens. Effect of Specimen Thickness. Doubly Logarithmic Plot	10
Fig. 6	Schematic of Phase Shift Generating Network.	11
Fig. 7	Schematic of Phasemeter Network.	11
Fig. 8	Plots of Calculated <u>vs.</u> Measured Phase Angles at Various Low Frequencies.	13
Fig. 9	Tilted Ellipse	14
Fig. 10	Static Compressibility Data Obtained at 25 and 50°C on Dioctyl Sebacate Compared with Data Obtained from the National Bureau of Standards	17
Fig. 11	Schematic Diagram Showing Major Features of Dynamic Compressibility Apparatus.	19
Fig. 12	Variations in Output and Phase Angle with Relative Position of Piston (Data Obtained in Dynamic Compressibility Apparatus with DC 330 Silicone Fluid and a Stainless Steel Plug in Cavity Covered by Mylar Diaphragm).	20
Fig. 13	Data Obtained under Conditions Similar to those in Fig. 12 with Mylar Diaphragm Replaced by Rubber Diaphragm.	22
Fig. 14	Data Obtained under Conditions Similar to those in Figs. 12 and 13 with only DC 330 Silicone Fluid in the Cavity (Rubber Diaphragm over Cavity)	23

TABLES

Table I	Static Shear Moduli G_0 (Corrected) and G (Uncorrected, Shown in Parentheses) of SBR Specimens of Varying Thickness and Area	4
Table II	Analysis of Variance of Uncorrected Static Shear Moduli G	4
Table III	Analysis of Variance of Corrected Static Shear Moduli G_0	4
Table IV	Static Shear Moduli G of Polyurethane Propellant AEBA-10 Specimens of Varying Thickness and Area.	6
Table V	Analysis of Variance of Static Shear Moduli G	6

I INTRODUCTION

An investigation of the viscoelastic properties of solid propellants and propellant binders, which has been conducted under Contracts NOW 61-1057-d and NOW 65-0073-d, is now being continued under Contract NOW 65-0061-d. This second Quarterly Technical Summary Report covers the period December 16, 1964 to March 15, 1965 and is the fourteenth report of the series. The objectives are to characterize the viscoelastic properties of propellants in shear, in tension, and under hydrostatic pressure (both static and oscillatory).

Studies which relate to the operation of the dynamic shear tester and to the resulting data are described in this report. Following the report period data were obtained on a polyurethane propellant over extended ranges of temperature and frequency; these data will be presented and discussed in subsequent reports. Progress on the dynamic compressibility apparatus is discussed, and compressibility data obtained with the static apparatus at 25 and 50°C on dioctyl sebacate are given.

Biaxial tests on a thin-walled cylinder of propellant are planned. The specimen will be tested in tension with its outer diameter maintained constant by admitting pressurized gas to the inside of the cylinder. The device for automatically regulating the required gas pressure has been constructed and preliminary tests have been made on cylinders of unfilled rubber. These tests showed that adequate control of the gas pressure can be maintained during a test at a constant rate of strain in the longitudinal direction.

II DYNAMIC SHEAR PROPERTIES

The effect of specimen dimensions on the static compressional moduli of SBR and polyurethane propellant AEBA-10 specimens were investigated using an improved method. A study was then made of the shear strain dependence of the dynamic moduli of the propellant specimens at one temperature and one frequency. Finally, the differential Lissajous method for the determination of small phase angles at low frequencies was definitely evaluated by measuring electronically produced phase angles which could be calculated precisely.

A. Static Shear Modulus of SBR

An attempt was made previously to assess the effect of specimen thickness on the static modulus of SBR using data collected while studying the effect of the compressive strain on the dynamic moduli. The results were reported in the Annual Technical Summary Report (No. 12 of series, dated October 15, 1964) and a theoretical discussion was given. It was then remarked that the data were not highly precise but that the measuring techniques had been improved so that data of better precision could be obtained.

This section reports on a more detailed study of the effect of specimen dimensions on the static compressional modulus of SBR specimens; the data were obtained by the improved method. The specimens were the rectangular blocks of SBR described in Technical Summary Reports No. 12 and 13 of the series. All measurements were carried out in the shear tester at ambient temperature. The measured compressive stress σ_c was plotted against $-(\lambda - \lambda^{-2})$ and the (uncorrected) static shear modulus G was obtained from the slopes of these plots according to the equation

$$\sigma_c = -G(\lambda - \lambda^{-2}) \quad (1)$$

(cf. p. 9 of the Annual Technical Summary Report, October 15, 1964). The plots for the 2.3-inch-long specimens are shown in Fig. 1. Table I shows the uncorrected static shear moduli in parenthesis next to the moduli obtained by using the Payne-Scott correction (cf. Eq. (20), p. 10, Annual Technical Summary Report, October 15, 1964). The uncorrected values decrease with increasing thickness and increasing area. As shown by the analysis of variance, presented in Table II, the variation due to thickness is very highly significant, but that due to area is not significant statistically when tested against the interaction as an estimate of error.

Table III shows the analysis of variance performed on the corrected moduli G_0 . Neither the variation due to thickness nor that due to area is now statistically significant at the 5% level against the interaction. The Payne-Scott correction therefore appears to reduce successfully the dependence of the static modulus on the geometrical factors. The static compressional modulus of the SBR may consequently be taken as 5.7×10^8 dynes/cm².

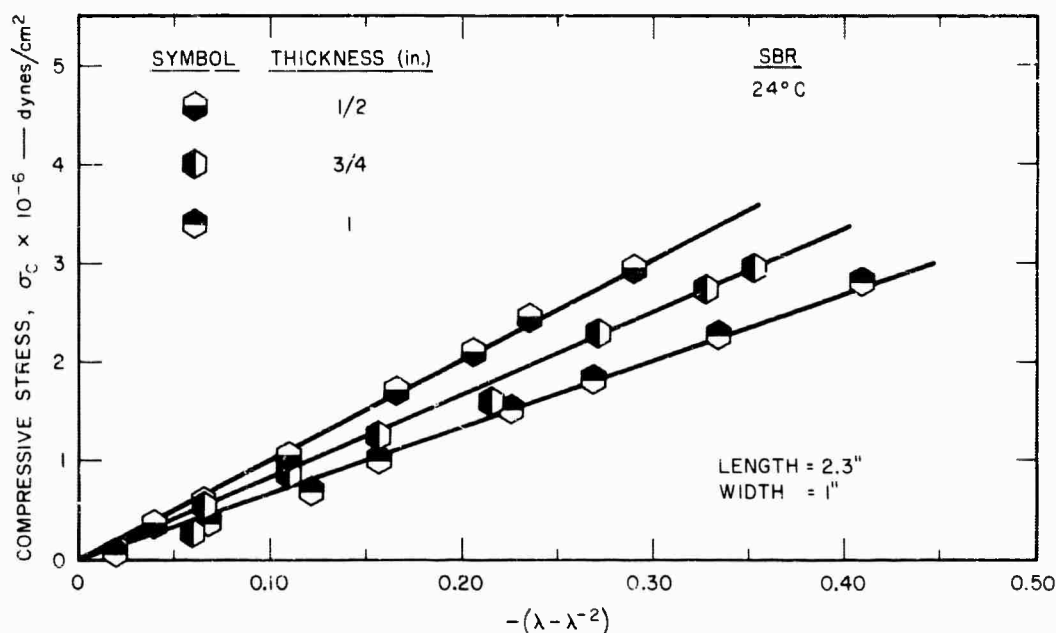


FIG. 1 PLOT OF COMPRESSIVE STRESS σ_c vs. $-(\lambda - \lambda^{-2})$ FOR SBR SPECIMENS

Table I

STATIC SHEAR MODULI G_o (CORRECTED) AND G (UNCORRECTED, Shown in Parentheses) OF SBR SPECIMENS OF VARYING THICKNESS AND AREA

Area (sq. in.)	Thickness (in.)			
	1/2	3/4	1	av.
1.0	6.26 (9.30)	5.94 (7.36)	6.06 (9.90)	6.09 (7.85)
2.3	5.96 (10.08)	5.72 (8.41)	5.06 (6.66)	5.58 (8.38)
3.0	5.64 (10.65)	5.20 (7.92)	5.38 (7.40)	5.41 (8.66)
av.	5.95 (10.01)	5.62 (7.90)	5.50 (6.99)	5.69 (8.30)

Table II

ANALYSIS OF VARIANCE OF UNCORRECTED
STATIC SHEAR MODULI G

S.V.	D.F.	S.S.	M.S.	V.R.
Area	2	1.00	0.50	2.63 ^{ns}
Thickness	2	14.43	7.21	37.9***
Interaction	4	0.76	0.19	
Total	8	16.19		

Table III

ANALYSIS OF VARIANCE OF CORRECTED
STATIC SHEAR MODULI G_o

S.V.	D.F.	S.S.	M.S.	V.R.
Area	2	0.7491	0.3745	5.90 ^{ns}
Thickness	2	0.3310	0.1655	2.61 ^{ns}
Interaction	4	0.2536	0.0634	
Total	8	1.3337		

B. Static Shear Modulus of Polyurethane Propellant AEBA-10

For this work the cylindrical and disk-shaped specimens described on p. 9 of the previous Quarterly Technical Summary Report (No. 13 of series) were used. The measurements were carried out in the shear tester at ambient temperature. Plots of the compressive stress σ_c against the compressive strain ϵ_c for the one-inch-diameter specimens are shown in Fig. 2. Similar plots were prepared for the other specimens. The slopes

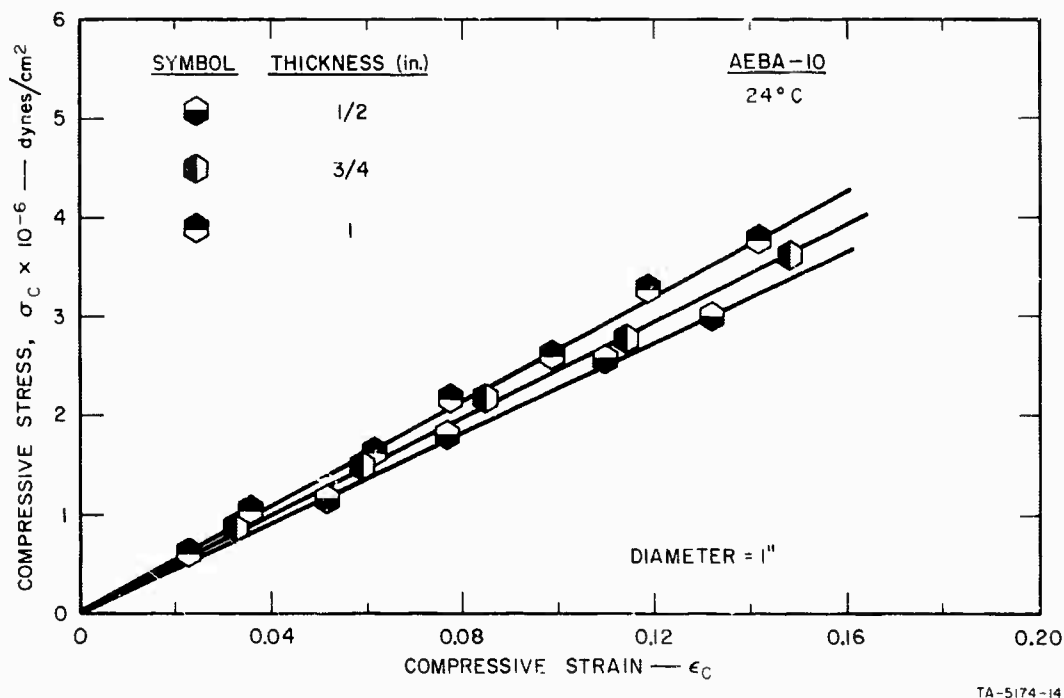


FIG. 2 PLOT OF COMPRESSIVE STRESS σ_c vs. COMPRESSIVE STRAIN ϵ_c FOR SPECIMENS OF POLYURETHANE PROPELLANT AEBA-10

of the straight lines drawn through the experimental points yield the static Young's modulus E from which the static shear modulus G is obtained ($G = E/3$). The values are tabulated in Table IV.

The variation of the modulus with specimen geometry is exactly opposite to that observed on the SBR specimens: The static shear modulus of the propellant increases with increasing thickness and decreasing

area. However, only the variation in area is statistically significant against the interaction as shown in Table V below.

Table .

STATIC SHEAR MODULI G OF POLYURETHANE
PROPELLANT AEBA-10 SPECIMENS
OF VARYING THICKNESS AND AREA

Area (sq. in.)	Thickness (in.)			
	1/2	3/4	1	av.
.44	9.09	8.25	9.09	8.81
.79	7.96	8.20	9.02	8.40
1.21	7.76	7.35	7.58	7.56
av.	8.28	7.93	8.56	8.26

Table V

ANALYSIS OF VARIANCE OF STATIC SHEAR MODULI G

S.V.	D.F.	S.S.	M.S.	V.R.
Area	2	0.5963	0.2982	2.07 ^{ns}
Thickness	2	2.4166	1.2083	8.38 [*]
Interaction	4	0.5765	0.1441	
Total	8	3.5894		

Values of G obtained from plots of σ_c vs $-(\lambda-\lambda^{-2})$ are somewhat lower but show, of course, the same general variation as those from the plots of σ_c vs ϵ_c . The Payne-Scott correction (cf. Annual Technical

Summary Report, October 15, 1964, p. 12) for circular specimens is

$$\Phi = 1 + B(D/h_0)^2 \quad (2)$$

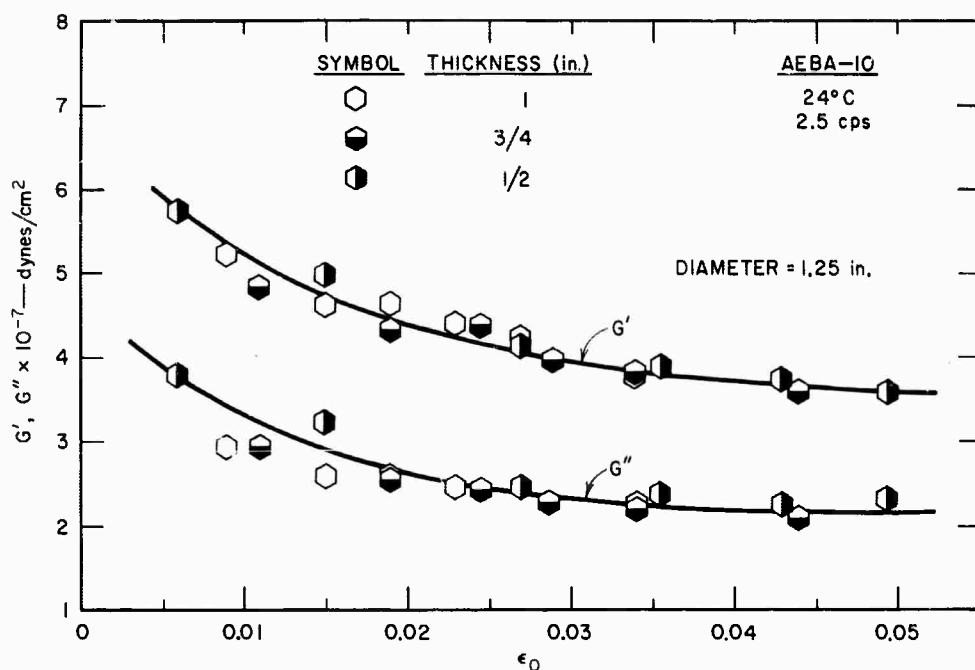
where $B = 0.120$ in this case, D is the diameter, and h_0 the thickness. It can readily be seen that this correction would only increase the observed variation instead of reducing it.

In Annual Technical Summary Report (No. 12, p. 22) measurements of the static compressional modulus were presented which were carried out on rectangular specimens of the same propellant. It was shown that these data could be corrected successfully by the use of the Payne-Scott equation. The observations reported here on the circular specimens are at variance with these results in that the Payne-Scott correction could not be applied. The reason for this difference is not known, but it should be noted that the area of the rectangular specimen (3 sq. in.) was larger than the areas of the circular specimens. No measurements were made on rectangular specimens with smaller areas and thus the statistical significance of the thickness variation could not be assessed.

C. Effect of Specimen Geometry and Cam Displacement
on Dynamic Shear Moduli

In Annual Technical Summary Report (No. 12 of series), it was shown that the storage and loss moduli of SBR specimens depended on the shear strain. Experiments were therefore carried out to obtain information on the shear strain dependence of the moduli of polyurethane propellant AEBA-10. As in the SBR experiments, the shear strain was varied by changing the cam displacement. Tape-bonded cylindrical specimens were used at a compressive strain of 0.05. The measurements were carried out at 2.5 cps at ambient temperature.

Figure 3 demonstrates the effect of specimen thickness on the shear strain dependence of the three 1.25-inch-diameter specimens. The effect



TA-5174-12

FIG. 3 SHEAR STRAIN DEPENDENCE OF THE STORAGE AND LOSS MODULI OF POLYURETHANE PROPELLANT AEBA-10 SPECIMENS.
Effect of specimen thickness

of specimen area (diameter) is shown in Fig. 4 for the 1-inch-diameter specimens. The other thicknesses and diameters gave very similar results. As with the SBR specimens, there is a definite dependence of the moduli on the shear strain. Contrary to the results obtained on the SBR specimens, however, the curves do not flatten out appreciably at shear strains higher than 0.02 (cf. p. 18, Annual Technical Summary Report).

Because of the compliance of the load cell, the shear strain experienced by the specimen is not directly proportional to the cam displacement but depends on the modulus of the test specimen and thus on the temperature and the frequency at which the test is made. For practical reasons it is not possible to work at a predetermined shear strain and some means must be found to correct data for a reference shear strain level.

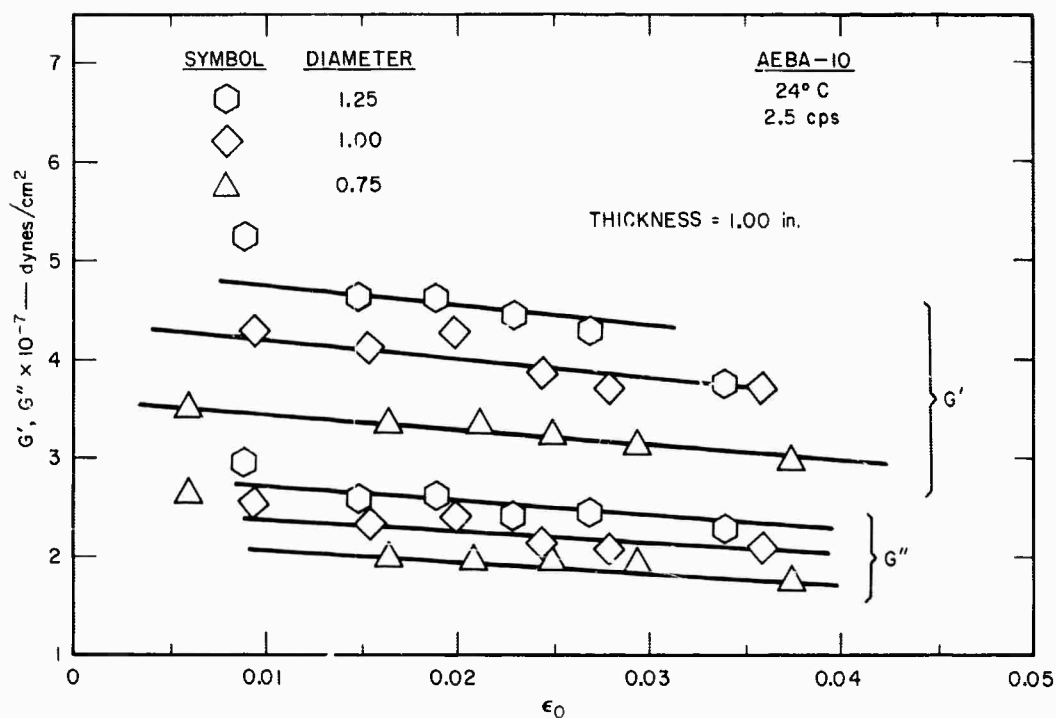


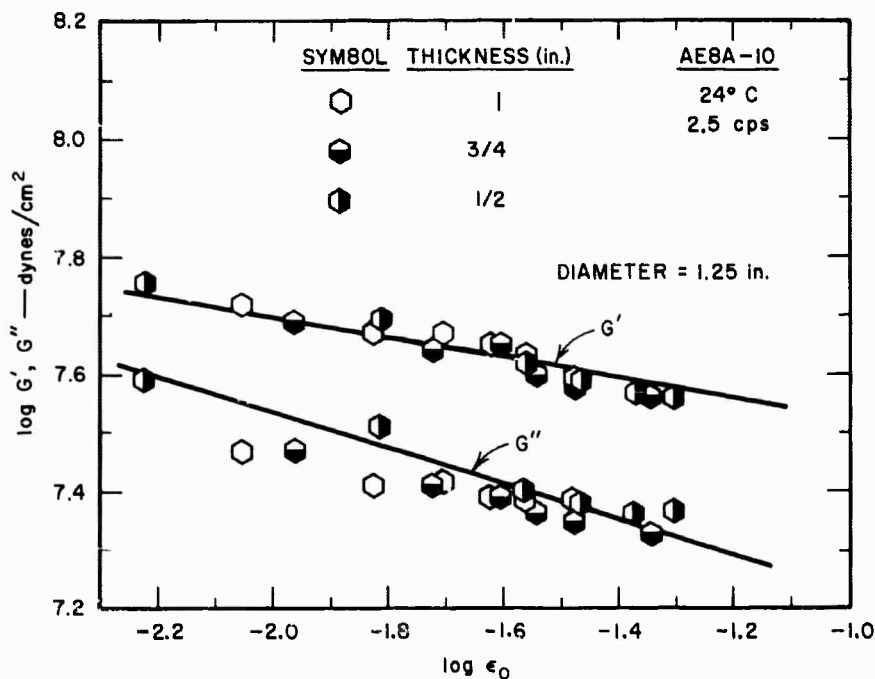
FIG. 4 SHEAR STRAIN DEPENDENCE OF THE STORAGE AND LOSS MODULI OF POLYURETHANE PROPELLANT AEBA-10 SPECIMENS.
Effect of specimen diameter

As shown in Fig. 5, a plot of $\log G'$ and $\log G''$ against $\log \epsilon_0$ yields a reasonable linearization of the behavior and is suitable for small corrections.

D. Differential Lissajous Method

In several previous reports, details were given of the development of the differential Lissajous method for measuring small phase angles at low frequencies. During the present report period this method was verified by measuring small phase angles which are known precisely.

In these measurements the peak amplitudes of the two signals were nearly equal. Proper leveling of the ellipse then depends on the correct handling of the base gain g_B . This was mentioned briefly in the Annual Technical Summary Report (No. 12 of series) and will here be discussed in more detail.



TA-5174-13

FIG. 5 SHEAR STRAIN DEPENDENCE OF THE STORAGE AND LOSS MODULI OF POLYURETHANE PROPELLANT AEBA-10 SPECIMENS. Effect of specimen thickness. Doubly logarithmic plot

1. Verification of the Method

The method of producing the known phase shift is shown diagrammatically in Fig. 6. A Hewlett Packard Model 202A Function Generator was used as the signal source. R_1 is a 500-ohm shunt resistance equal to the output impedance of the generator which thus operates at design load. R_1 is also used for fine regulation of the signal amplitude. The signal is split, one portion being fed to the F (force) terminal of the phase-meter network shown in Fig. 7, while the other portion goes to a phase shifting network consisting of a general Radio Corp. Model 1432-P Decade Resistance Box (1,111,100 ohms total, in steps of 10 ohms) and a 1.0006 μF fixed capacitor C whose capacitance was determined precisely in a capacitance bridge. The phase-shifted signal is then passed through a Burr-Brown Model 1507 operational amplifier to the X (displacement) terminal of the phasemeter network. The amplifier serves as a convenient impedance-matching device and effectively isolates the two signals.

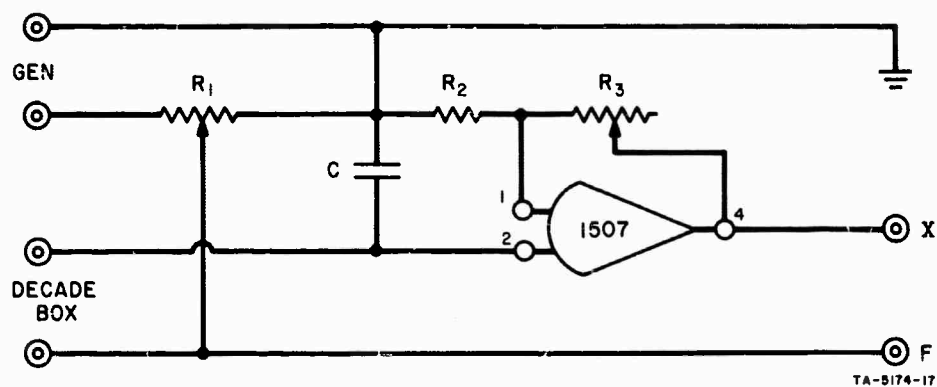


FIG. 6 SCHEMATIC OF PHASE SHIFT GENERATING NETWORK

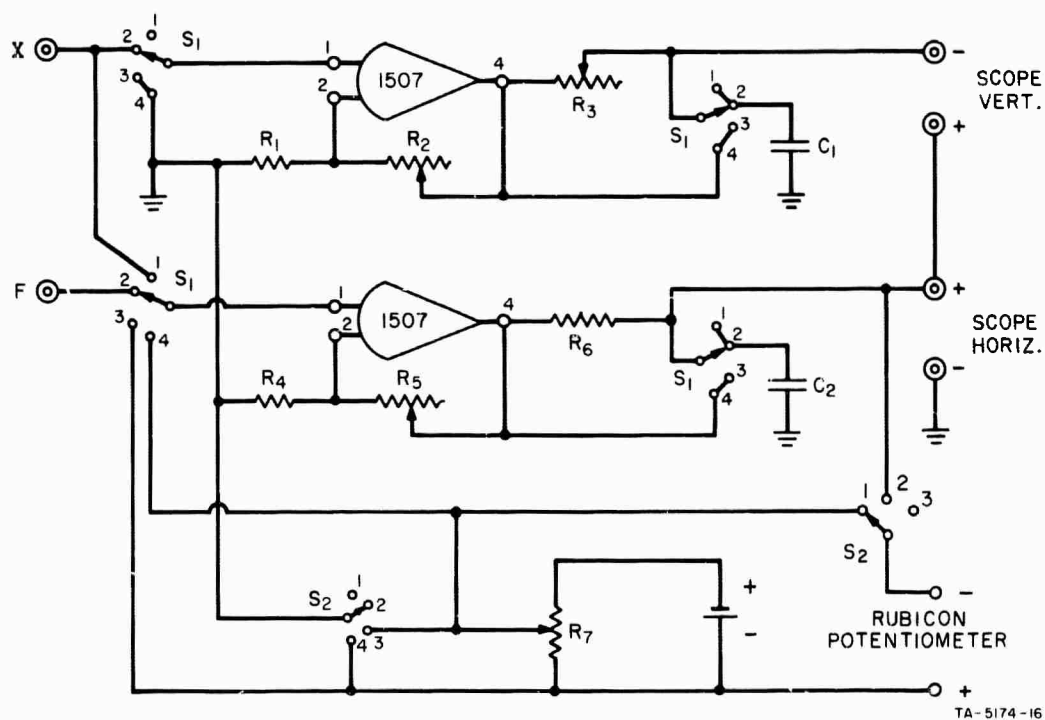


FIG. 7 SCHEMATIC OF PHASEMETER NETWORK

The phase shift between the two signals is then obtained as the ratio between the imaginary and real parts of the transfer function of the phase shifting network. The transfer function

$$g_p = 1/(1 + j\omega CR) \quad (3)$$

and consequently

$$\tan \phi = |\text{Im } g_p / \text{Re } g_p| = \omega CR. \quad (4)$$

The phase angle as measured by the differential Lissajous method is obtained (cf. p. 4, Quarterly Technical Summary Report No. 11), as

$$\sin \phi = d_D g_D / d_X g_X \quad (5)$$

where d_X is the peak X-signal and d_D the peak difference signal (the minor axis of the leveled ellipse) in centimeters as measured on the oscilloscope screen and g_D and g_X are the scope amplifier sensitivities (in mV/cm) used in recording the two signals.

Figure 8 shows plots of measured vs calculated phase angles at various frequencies. The measured angles are plotted on the ordinates as $\sin \phi$ while the calculated angles are plotted on the abscissa as $\tan \phi$. The straight lines represent the theoretical relationship between $\sin \phi$ and $\tan \phi$ which are identical for these low angles. Evidently at frequencies as low as 0.25 cps, phase angles of the order of only a few thousandths of a radian can be measured with very good precision. The lowest frequency at which measurements were attempted was 0.05 cps and even at this frequency the precision was excellent.

2. The Role of the Base Gain

In the differential Lissajous method, the difference between the two signals (F-X, say) is fed to the vertical amplifier of an oscilloscope while the weaker of the two (F, say,) is led to the horizontal amplifier. In general the major axis of the resulting ellipse will

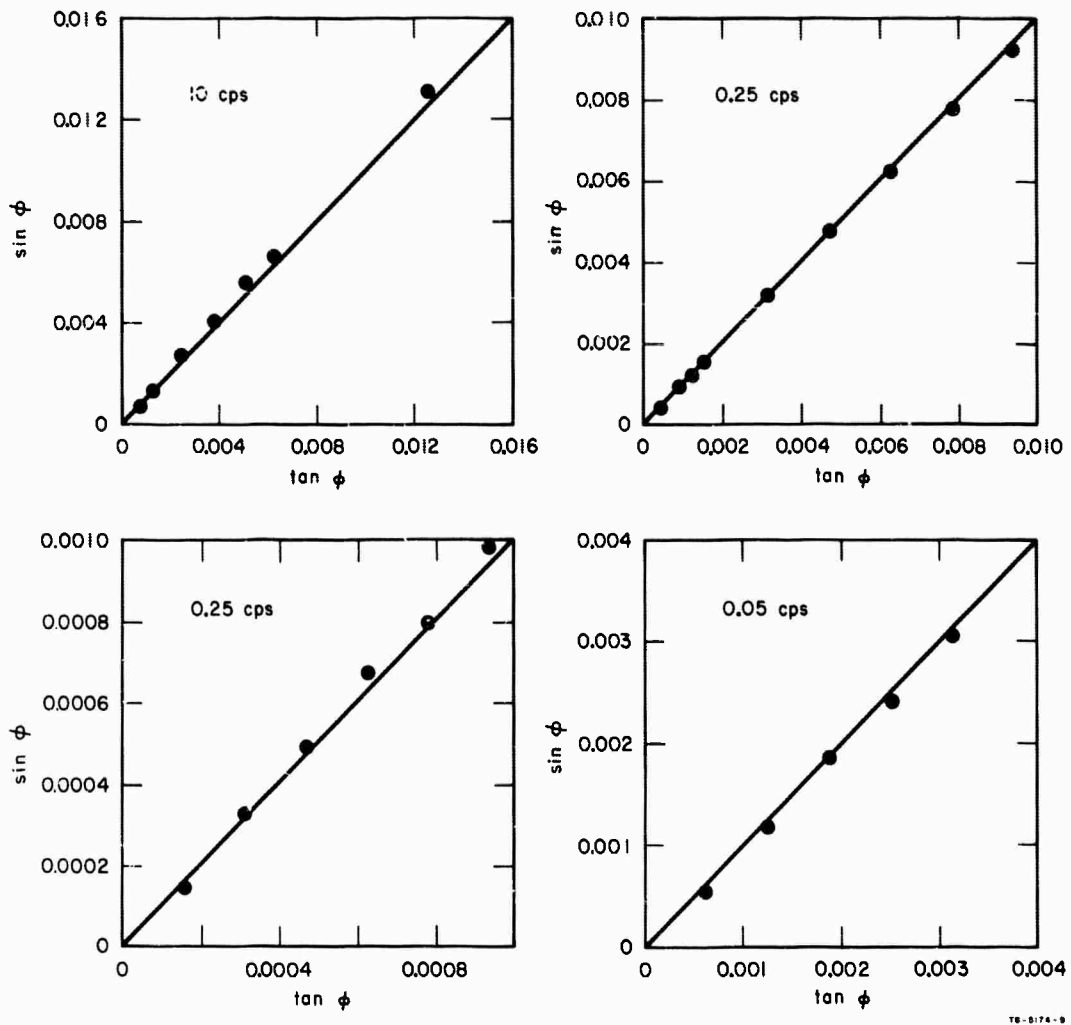


FIG. 8 PLOTS OF CALCULATED vs. MEASURED PHASE ANGLES
AT VARIOUS LOW FREQUENCIES

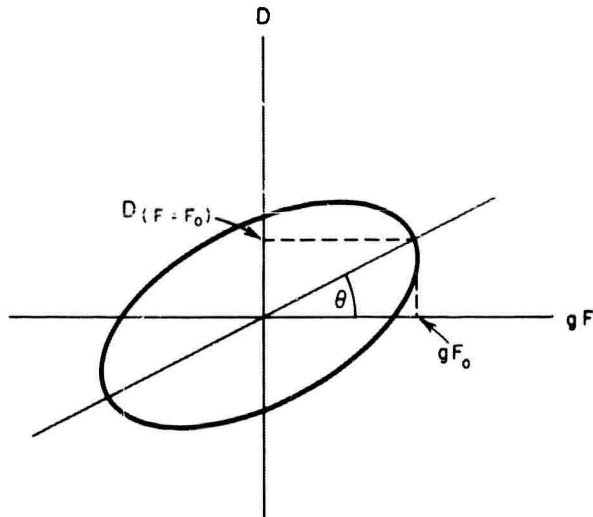
form an angle θ (the angle of tilt) with the horizontal axis of the oscilloscope screen as shown in Fig. 9. The difference signal arriving at the vertical amplifier is

$$D = gF_0 \sin (\omega t + \phi) - X_0 \sin \omega t \quad (6)$$

while the signal at the horizontal amplifier becomes

$$gF = gF_0 \sin (\omega t + \phi) \quad (7)$$

since this signal passes through an operational amplifier with variable gain g .



TA-5174-23

FIG. 9 TILTED ELLIPSE

The angle of tilt of the ellipse is

$$\tan \theta = D(F = F_0)/gF_0. \quad (8)$$

For F to achieve its peak value F_0 , $\omega t + \varphi$ must equal $\pi/2$, and therefore

$$D(F = F_0) = gF_0 - X_0 \sin(\frac{\pi}{2} - \varphi) = gF_0 - X_0 \cos \varphi.$$

Substituting into Eq. (8)

$$\tan \theta = 1 - X_0 \cos \varphi / gF_0$$

Proper leveling of the ellipse can only be achieved if the ellipse can be rotated through zero angle of tilt so that the level position can be approached from both sides. We can distinguish three cases:

1. If $F_0 < X_0 \cos \varphi$, the angle of tilt will be negative for $1 < g < X_0 \cos \varphi / F_0$, zero for $g = X_0 \cos \varphi / F_0$, and positive for $g > X_0 \cos \varphi / F_0$. The ellipse can therefore be rotated through zero tilt.

2. If $F_0 = X_0 \cos \varphi$, the angle of tilt is zero for $g = 1$, and positive for $g > \cos \varphi$. It can never be negative since $g > 1$. The ellipse can be leveled but it cannot be rotated through zero tilt.

3. If $X_0 \cos \varphi < F_0 < X_0$, the angle of tilt is always positive and the ellipse cannot be leveled at all.

To insure the proper rotation of the ellipse in cases (2) and (3) an arbitrary "base gain" g_B can be introduced into the X-path by the proper adjustment of the feedback loop of the operational amplifier in this path. The equation for the angle of tilt then becomes

$$\tan \theta = 1 - g_B X_0 \cos \varphi / g F_0$$

and, provided $g_B > 1/\cos \varphi$, it will always be possible to rotate the ellipse through zero tilt. The extent of the negative tilt depends on the magnitude of g_B . In normal operation one would expect an angle of 45° to be the largest to be measured by this method. One finds

$$\cos \varphi = \cos \pi/4 = 1/\sqrt{2}$$

i.e., g_B should not be less than $\sqrt{2}$. Making $g_B = 2$ is the logical choice and should be adequate for most cases.

The operating procedure is as follows. With switch S1 in position 4 and switch 2 in position 1, R_7 is regulated until a convenient mV output is read on the Rubicon potentiometer. S2 is then switched into position 2 and R_5 is regulated until the mV reading on the Rubicon potentiometer is exactly twice (for $g_B = 2$) the previous reading. It should be noted that when S1 is in position 4, the input to the X-amplifier is grounded and the F-filter ($R_6 - C_2$) is switched out of the F-path.

S1 is now put into position 1 and R_2 and R_3 are adjusted while the ellipse is leveled (R_2) and collapsed (R_3) into a straight line. At this point the gain and phase shift through the X- and the F-path at the given frequency are identical, and the phasemeter network is in the correct condition for recording the measurements from which the amplifier ratio and phase angle between the X- and the F-signal are obtained. This procedure is detailed in the Annual Technical Summary Report (No. 12 of series).

III DEPENDENCE OF SPECIFIC VOLUME ON PRESSURE, TEMPERATURE, AND TIME

In previous work, the static compressibility of two propellants and one propellant binder was determined over an extended range of temperature and at pressures up to 1500 psi. Some information was also obtained on the dependence of specific volume on temperature and time at atmospheric pressure. The results have been presented in previous reports and the conclusions are summarized in the Annual Technical Summary Report (No. 12 in series).

Because of certain operational limitations of the static bulk compressibility apparatus, a new apparatus was constructed and is now being evaluated. A schematic of the new apparatus is shown in Quarterly Technical Summary Report, No. 10 in the series. The instrument, based on hydrostatic weighing with an electrobalance, is designed to operate at pressures up to 3000 psi and at temperatures from -60° to $+60^{\circ}\text{C}$.

To determine the dependence of compressibility on pressure, temperature, and frequency, a dynamic compressibility apparatus has also been developed and currently is being evaluated. This apparatus was designed to operate at frequencies between 0.01 and 1000 cps, at static pressures up to 2000 psi and at temperatures between -60° and $+60^{\circ}\text{C}$. A description of the apparatus is given in Quarterly Technical Summary Report No. 10.

A. Static Compressibility

The static compressibility apparatus was evaluated during the present report period by determining the pressure dependence of the density of dioctyl sebacate at two temperatures. Dioctyl sebacate was selected because density-pressure data on this fluid have been provided by J.E. McKinney of the National Bureau of Standards.

Densities were determined using a pyrex plummet whose volume at 25°C was 0.5 ml. Helium was used as the pressurizing gas. In Fig. 10 the resulting data are compared with those from NBS. At 50°C, the two sets of data are sensibly identical, whereas at 25°C the NBS data lie somewhat below our data. However, the difference is quite small and within the experimental error. Data at both temperatures gave bulk compressibilities which are in excellent agreement with those from NBS. As seen in Fig. 10, the density at high pressures increases nonlinearly with pressure, especially at 25°C.

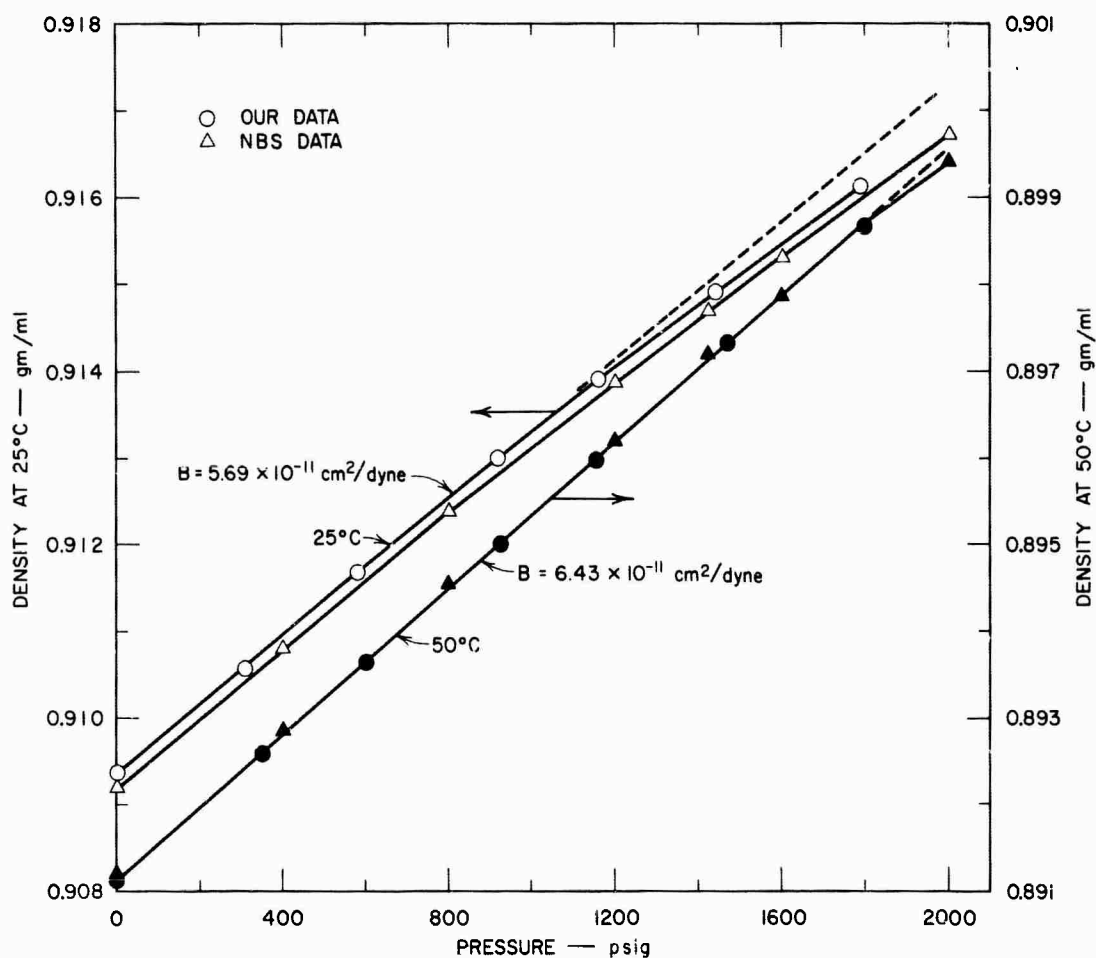


FIG. 10 STATIC COMPRESSIBILITY DATA OBTAINED AT 25 AND 50°C ON DIOCTYL SEBACATE COMPARED WITH DATA OBTAINED FROM THE NATIONAL BUREAU OF STANDARDS

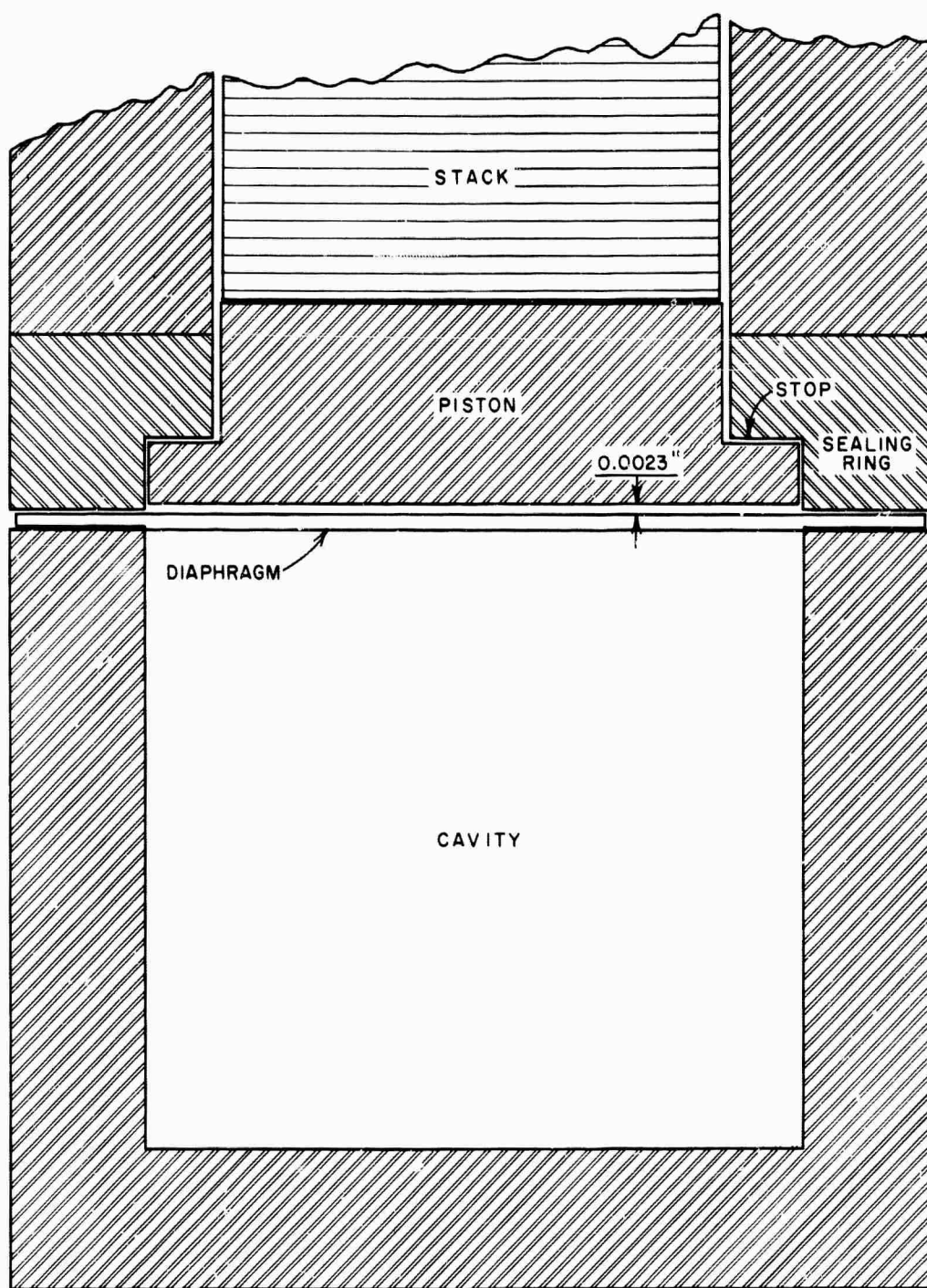
The apparatus functions quite satisfactorily, although a shift in the zero occasionally occurs during pressurization; the reason for the shift is not known. Due to the extreme sensitivity of the apparatus, temperature must be controlled very precisely. Thus, after the pressure has been changed, weighings are made only when a thermocouple indicates that the original temperature has been re-established.

Several check runs on the dioctyl sebacate at low temperatures are planned. Subsequently, data will be obtained on a propellant specimen.

B. Dynamic Bulk Compressibility

A series of calibration runs on the dynamic compressibility apparatus was completed. The resulting data showed that the transducer and apparatus constants, K' , K'' , B'_C , and B''_C (c.f. Quarterly Technical Summary Report, No. 10 of the series) varied by about $\pm 15\%$ from run to run. The calibration data showed that factors other than a variation in output of the crystal stack with static load were involved. It was concluded that the lack of reproducibility may be caused by a variation in the relative position of the piston which is driven by the crystal stack. The position of the piston is determined by (1) the initial static load imposed when the pressure plug is screwed into the apparatus, and (2) the displacement of the stack and the threads when the static pressure is changed. A change in temperature also changes the static pressure and thus the position of the piston.

In an attempt to evaluate these factors, the pressure plug was equipped with a pointer to measure the degrees of rotation and hence the linear displacement which occurs in the stack-piston assembly when the plug is inserted and tightened. To determine the yield of the stack and of the pressure vessel threads under compressive load, several special tests were made on components of the apparatus. To have a reproducible starting point, all runs made with the assembled apparatus were started with the piston in contact with the protective stop of the sealing ring (see Fig. 11). The electric output was measured, at a constant driving



TA-5174-1B

FIG. 11 SCHEMATIC DIAGRAM SHOWING MAJOR FEATURES
OF DYNAMIC COMPRESSIBILITY APPARATUS

voltage, for different positions of the piston; the position was calculated from the amount of rotation of the pressurizing plug and the known yield of the stack and the threads. Figure 12 shows some typical results obtained at 1000 psig and 1000 cps when the cavity contains the silicone DC 330 fluid and a steel plug. (The piston position indicated is relative to the stop on the sealing ring). The maximum output at about 2.25 thousandths of an inch corresponds approximately to the condition that would result if the piston in Fig. 10 were moved down until it contacts the diaphragm. At this point, the contact area between the piston and the diaphragm is a maximum. In this position, the phase angle is a minimum, although it increases rather suddenly on either side of the 2.25 thousandths point. Similar results were obtained at other frequencies and pressures.

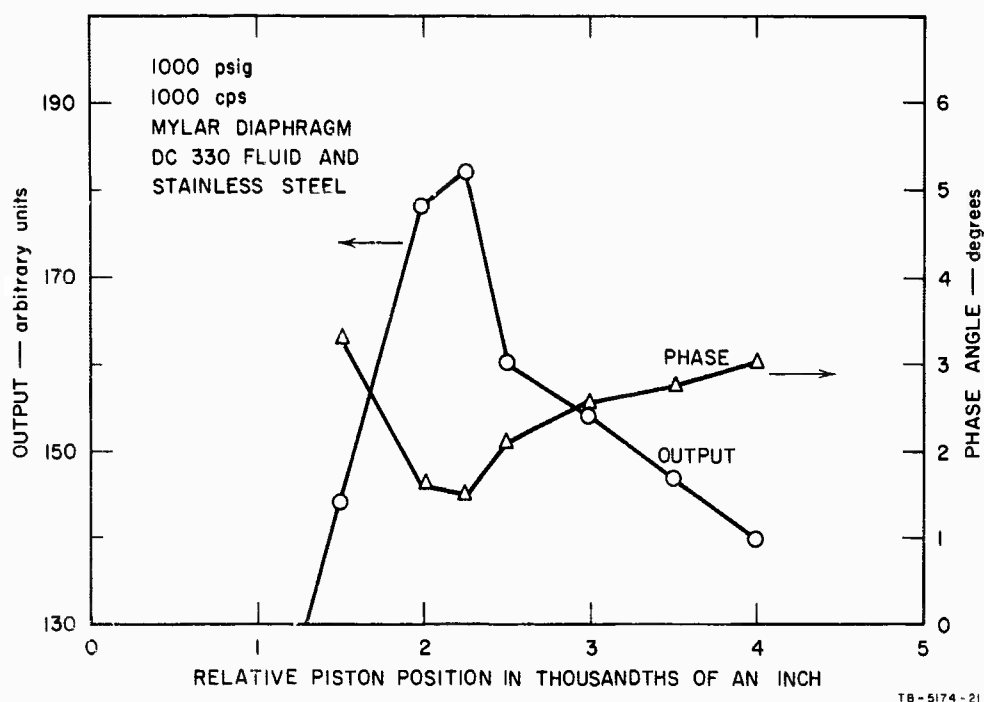


FIG. 12 VARIATIONS IN OUTPUT AND PHASE ANGLE WITH RELATIVE POSITION OF PISTON
(Data obtained in dynamic compressibility apparatus with DC 330 silicone fluid and a stainless steel plug in cavity covered by Mylar diaphragm)

These data are interpreted as follows. At the 2.25 thousandths displacement, the piston contacts the entire area of the diaphragm. Below the 2.25 thousandths position, the contact area is reduced somewhat due to the inability of the diaphragm to conform completely to the periphery of the piston. Above the 2.25 thousandths position, the piston forces the diaphragm into the cavity. Loss of electrical output in the latter situation may be due to two factors: (1) lack of contact in the center of the diaphragm; and (2) reduced motion due to the restriction at the periphery of the piston. Since phase angles result from any loss of energy, the increase in phase angle on either side of the 2.25 thousandths position may result from compression of air between the piston and the diaphragm and from energy dissipated in the peripheral area.

As the piston position changes with static pressure due to the yield, the output and the phase angle should vary in a predictable manner with cavity pressure for a given initial positioning of the piston. Tests at various initial positions of the piston showed the predicted variation, e.g., increasing the cavity pressure moves the output to the left on the curve in Fig. 12.

To determine whether the results depend on the properties of the diaphragm, the Mylar diaphragm was replaced by a soft rubber one of approximately the same thickness. As the rubber should deform more readily and give maximum contact area, it was felt the maximum electrical output would be less dependent on the piston position. Figure 13 shows that the output is now less sensitive to piston position, as expected. Surprisingly, the maximum output and minimum phase angle results at 4 thousandths displacement instead of the 2.25 obtained with the Mylar. Also, the maximum output is about 32% of that obtained with the Mylar. This lower output may result from the greater compressibility of the rubber diaphragm.

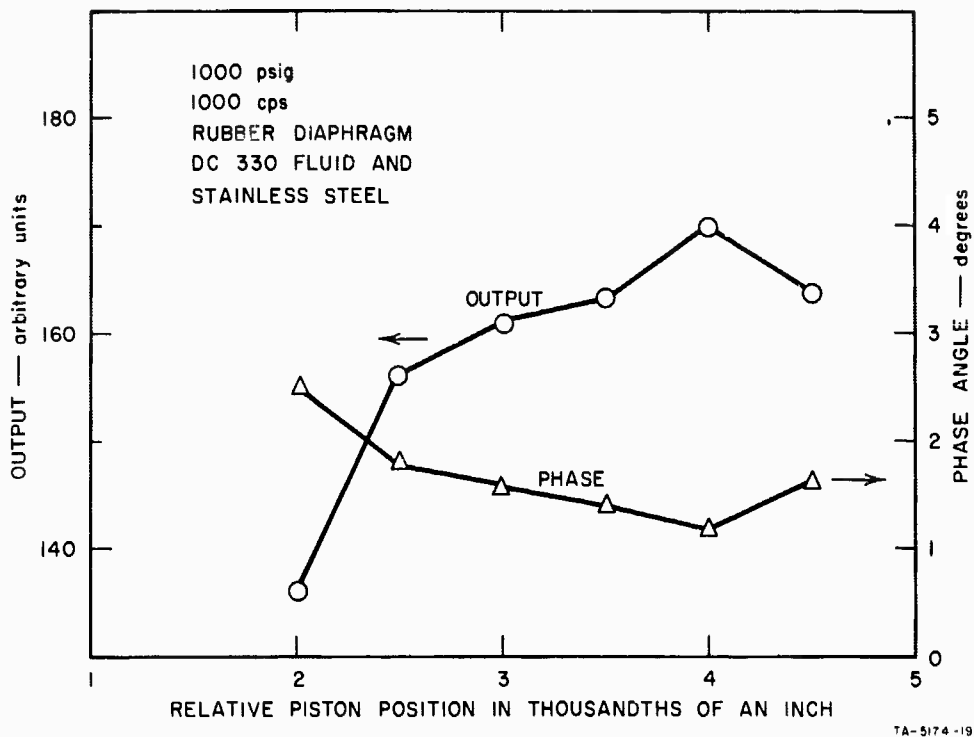


FIG. 13 DATA OBTAINED UNDER CONDITIONS SIMILAR TO THOSE IN FIG. 12 WITH MYLAR DIAPHRAGM REPLACED BY RUBBER DIAPHRAGM

Figure 14 shows data obtained with the rubber diaphragm but with the cavity containing only the DC 330 fluid. Maximum output is now at 2.5 thousandths, and the output curve resembles that obtained previously with the Mylar diaphragm. However, the phase angle now is a maximum when the output is maximum. A satisfactory explanation of these results is not apparent.

There can be little doubt that the lack of reproducibility is due to the position of the piston and the configuration of the diaphragm. The high precision required in the positioning operation makes it fairly difficult to obtain reproducible results. Several possible solutions to this problem are now being explored.

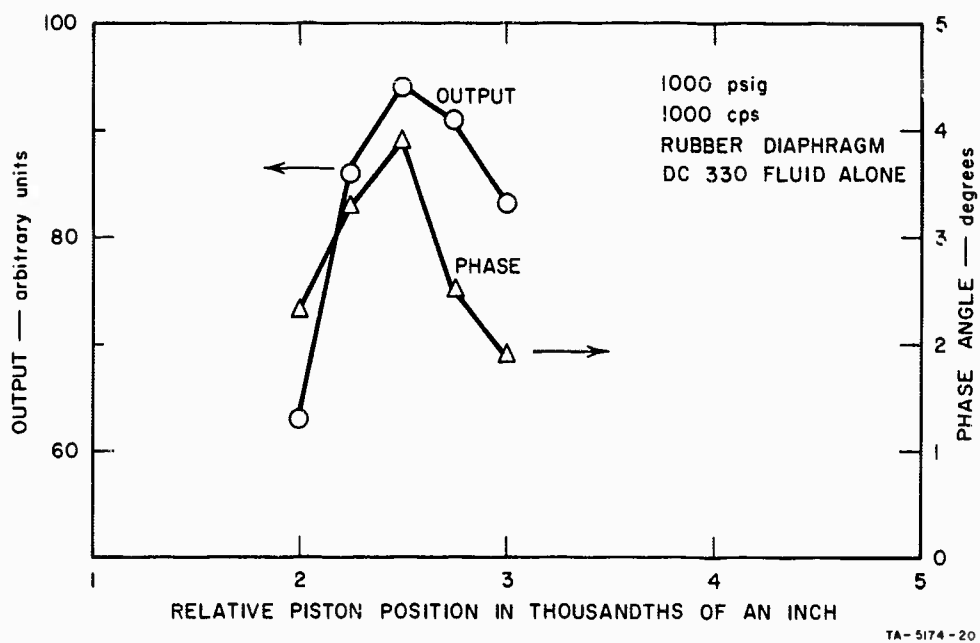


FIG. 14 DATA OBTAINED UNDER CONDITIONS SIMILAR TO THOSE IN FIGS. 12 AND 13 WITH ONLY DC 330 SILICONE FLUID IN THE CAVITY (Rubber diaphragm over cavity)

THIS REPORT HAS BEEN DELIMITED
AND CLEARED FOR PUBLIC RELEASE
UNDER DOD DIRECTIVE 5200.20 AND
NO RESTRICTIONS ARE IMPOSED UPON
ITS USE AND DISCLOSURE.

DISTRIBUTION STATEMENT A

APPROVED FOR PUBLIC RELEASE;
DISTRIBUTION UNLIMITED.